INSTITUTE OF PHYSICS PUBLISHING PLASMA SOURCES SCIENCE AND TECHNOLOGY

Plasma Sources Sci. Technol. **11** (2002) 439–447 PII: S0963-0252(02)52604-9

Two-photon laser induced fluorescence spectroscopy performed on free nitrogen plasma jets

S Mazouffre[1], I Bakker[2], P Vankan[2], R Engeln[2,3] and D C Schram[2]

[1] Laboratoire d'Aérothermique, CNRS, 1C avenue de la Recherche Scientifique, 45071 Orléans Cedex 2, France

[2] Department of Applied Physics, Centre for Plasma Physics and Radiation Technology, Eindhoven University of Technology, PO Box 513, 5600 MB Eindhoven, The Netherlands

E-mail: r.engeln@phys.tue.nl

Received 22 May 2002, in final form 9 August 2002
Published 2 October 2002
Online at stacks.iop.org/PSST/11/439

Abstract

The properties of free nitrogen plasma jets are examined by studying the ground-state nitrogen atom flow characteristics. The plasma is created by a cascaded arc and subsequently it expands freely into a low pressure vessel. In such a way supersonic flows with high Mach number are achieved. N(^{4}S) atoms are locally probed by means of two-photon absorption laser induced fluorescence spectroscopy. Axial and radial N(^{4}S) atom temperature and velocity profiles present the shape predicted by the neutral gas supersonic expansion theory. The adiabatic exponent γ is equal to 1.45 in the supersonic domain. A Mach number M of 4.4 is measured ahead of the normal shock wave. In contrast, density profiles reveal a departure from the classical expansion picture. Too small density jumps over the shock region indicate a non-conservation of the N(^{4}S) atom forward flux. Moreover the partial N(^{4}S) atom static pressure decreases in the subsonic domain. Loss of nitrogen atoms during the plasma expansion is a direct consequence of plasma–wall interactions. However, losses are limited because of the relatively high N atom mass and because of a low surface recombination probability of N atoms. The dissociation degree at the arc exit is around 40%. Under such circumstances N_2(A) molecules cannot survive in the jet. The local electron density is estimated from a measure of the radiative lifetime of the nitrogen atom excited state.

1. Introduction

Nitrogen and nitrogen-containing plasmas are already used for a variety of applications. In the field of surface treatments, such plasmas are widely employed for modifying specific surface properties, e.g. wettability or hardness, of metals and polymers (see the list of references in [1]). In the astronautics area, nitrogen plasma jets are used to study energy transfer to the surface of a space vehicle that occurs during the entry stage in the Earth's atmosphere [2, 3]. The list of well-established utilizations of nitrogen plasmas is long and several other examples can be given. However, an entirely new domain of applications is emerging nowadays. Indeed, nitrogen-containing semiconductors like GaN-based alloys offer the promise of major improvements in the performance of opto-electronic devices because of their wide bandgap and strong chemical bond. Applications such as blue-light emitting diodes [4], laser diodes and sensitive solar blind photo-detectors are currently under development [5]. Moreover, a material like SiN appears to be very suitable as anti-reflection coating for high conversion efficiency solar cells [6].

This set of novel applications requires the development of low cost plasma sources capable of providing high flux

[3] Author to whom correspondence should be addressed.

of atomic radicals. As very reactive species, nitrogen atoms play a major role in all chemical reactions that concern nitrogen plasmas, like direct surface modification via adsorption/diffusion processes or formation of precursor molecules in the gas phase. A high particle velocity is necessary to obtain a large flux of N atoms in order to speed up the overall chemistry. Supersonic plasma jets, which result from the expansion of a high pressure plasma into a low pressure environment, so-called free plasma jets, fulfil all the aforementioned requirements. Hence they are well suited for fast deposition of N-based semiconductors. Furthermore, the low ion content of such jets combined with a relatively low temperature warrants a low damage of the exposed surface. There is therefore a clear need to characterize the chemical potential of the jet in terms of active species content and flow properties. Several experimental works have already been devoted to the study of free nitrogen plasma jets. In the works conducted by Vervish *et al* a dc arc nitrogen plasma jet is investigated by means of emission spectroscopy and electrostatic probes. The measured N_2^*, N_2^{+*}, N^* and electron [7] density and temperature are compared with the outcome of a fluid model accounting for non-equilibrium effects [8]. Radial density profiles of ground-state N atoms, the most populated state in a low temperature plasma, and N(^{2}D,^{2}P) atoms are obtained from VUV absorption measurements [9]. The work of De Benedictis *et al* deals with RF nitrogen plasma jets. In these studies, optical emission spectroscopy is used to determined the particles velocity and temperature. Local measurements of the relative N(^{4}S) density are performed by means of a two-photon absorption laser induced fluorescence (TALIF) technique [10], and an estimate of the mean N(^{4}S) density is obtained from a titration with NO [11]. In a recent study performed by Douai *et al*, the nitrogen atom concentration is measured in expanding surface wave plasmas by means of modulated beam mass spectroscopy [12].

In this paper we present a TALIF spectroscopic investigation of nitrogen thermal plasma expansions generated by a cascaded arc. We describe measurements of the N(^{4}S) atom density, velocity and temperature performed in both radial and axial direction, and we discuss in detail the nitrogen atom flow pattern and the influence of wall-processes upon the nitrogen atom transport properties.

2. Expanding thermal nitrogen plasma

The nitrogen plasma is created by a cascaded arc [13]. The arc channel is composed of four insulated plates and has a diameter of 3 mm. The operating standard conditions are: a 55 A direct current (dc), a cathode–anode voltage of 120 V and a N_2 gas flow of 1.5 standard liters per minute (slm). The stagnation pressure inside the arc is 0.44 bar. The thermal nitrogen plasma expands from a straight nozzle with a diameter of 3 mm into a roots-blower pumped vacuum vessel (length 3 m, diameter 0.36 m) where the background pressure (p_{back}) can be varied, almost independently from the gas flow, from 5 Pa to atmospheric pressure. The cascaded arc plasma source is mounted on a translation arm. Spatial scans through the expanding plasma can be performed by moving the arc relative to the intersection of laser beam and detection volume.

The main topic of this paper is the study of the transport of ground-state nitrogen atoms in a plasma expansion. Therefore it is of interest to briefly discuss the ways N(^{4}S) atoms are created in the cascaded arc channel where the electron temperature T_e is around 1 eV. Nitrogen atoms can naturally be produced by direct dissociation of ground-state N_2 molecules by electron impact

$$N_2(X) + e \rightarrow N(^4S) + N(^4S) + e \qquad k \approx 10^{-16}\,\mathrm{m^3\,s^{-1}}\ \ [9]. \tag{1}$$

Nevertheless, at such a low T_e, other mechanisms are involved in the generation of N(^{4}S) atoms. The charge exchange reaction between N^+ and N_2(X) followed by the dissociative recombination of the formed molecular ion is also a very favourable process

$$N^+ + N_2(X) \rightarrow N(^4S) + N_2^+ \qquad k \approx 10^{-16}\,\mathrm{m^3\,s^{-1}}\ \ [14], \tag{2}$$

$$N_2^+ + e \rightarrow N(^4S) + N(^4S) \qquad k \approx 10^{-13}\,\mathrm{m^3\,s^{-1}}\ \ [15]. \tag{3}$$

Another possibility is the interaction between vibrationally excited nitrogen molecules $N_2(X, v)$ and electrons or excited N_2 molecules. Yet this channel requires a large amount of $N_2(X, v)$ molecules to be an efficient mean of N(^{4}S) production, which *a priori* is unlikely under our conditions. Notice that in the arc channel, as well as at the beginning of the nozzle, part of the atomic population can be stored in the form of metastable N(^{2}P) and N(^{2}D) atoms due to electron impact on N(^{4}S) and on N_2(X) [9] and due to recombination of molecular ions. However, in the final part of the nozzle and in the expansion, the electron density becomes rapidly to small too ensure a coupling between N ground-state and N excited states. Furthermore, remaining atoms in metastable states are quickly destroyed by collisions with N(^{4}S), N_2 molecules and the nozzle wall. A more complete review of nitrogen plasma kinetics can be found in [15–17].

A detailed description of the dynamics of a plasma expansion can be found elsewhere [18–20]. Here only a short overview of the expansion picture is presented. Because the plasma expands through a nozzle from a high pressure region into a low pressure region, a well defined free jet shock wave structure is produced, as schematically depicted in figure 1. The plasma first expands supersonically. At some distance from the source, a stationary normal shock wave is formed to allow the flow to adapt to the ambient gas conditions. Throughout the shock region the flow undergoes a transition from a supersonic regime to a subsonic regime. The Mach disc, location at which the Mach number M equals 1, defines the end of the shock wave. Behind the normal shock wave, the plasma flows subsonically and at constant static pressure. The supersonic domain is surrounded by a so-called stationary barrel shock wave.

3. TALIF spectroscopy of nitrogen atoms in free plasma jets

In the experiments reported in this contribution, the local macroscopic properties of ground-state nitrogen atoms are monitored by means of TALIF spectroscopy [1, 21, 22]. A simplified scheme of the experimental set-up is depicted

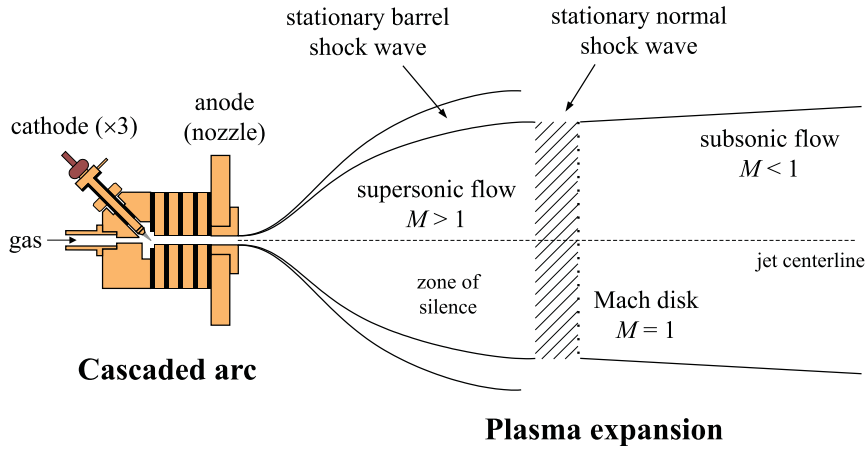

Figure 1. The cascaded arc and simplified structure of an expanding plasma jet. The plasma first expands supersonically from a straight nozzle. At some distance from the source a normal shock wave is created to allow the flow to adapt to the local conditions. Behind the normal shock front the plasma flows subsonically and at constant static pressure. The supersonic flow domain is limited by a barrel (side) shock wave. M refers to the Mach number.

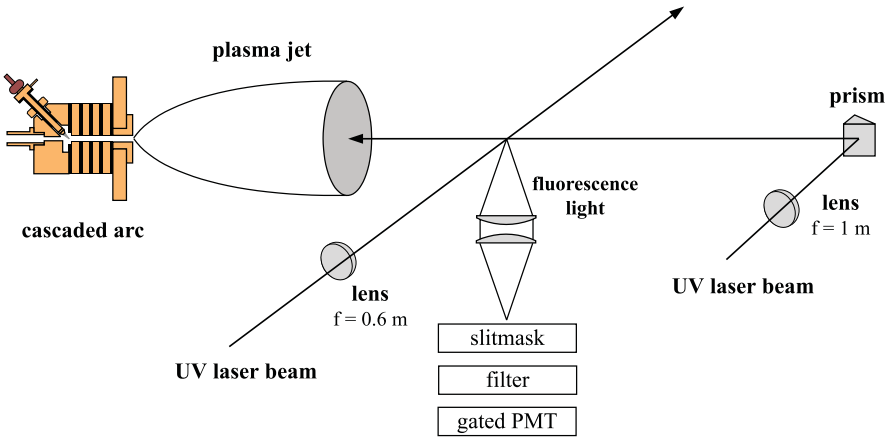

Figure 2. Schematic view of the experimental arrangement used to spatially probe ground-state nitrogen atoms by means of TALIF spectroscopy. The UV laser beam can be directed either perpendicular or parallel to the plasma jet axis, which allows for the measurement of $(T_\perp, v_r)$ and $(T_\parallel, v_z)$, respectively. The cascaded arc is mounted on a translation arm and therefore it can be moved in the 3 directions of space relative to the fixed detection volume.

in figure 2. A tunable 20 Hz Nd : YAG pumped dye laser (Spectra-Physics Quanta Ray GCR230/Sirah Cobra-Stretch combination) delivers radiation around 621 nm. The output of the dye laser is frequency-tripled using non-linear optical crystals resulting in 5 ns pulses of vertically polarized coherent UV light around 207 nm with a pulse energy up to 3 mJ and an estimated bandwidth of $0.12\,\mathrm{cm}^{-1}$ (note that during all experiments a pulse energy around $130\,\mu$J is used in order to avoid parasitic effects [22]). A set of high reflectivity dielectric mirrors is employed to separate the UV beam from the remaining blue and red beams. The two crystals are automatically angle tuned using a predetermined angle trajectory (passive tracking) to provide a constant output energy while scanning the dye laser wavelength. The UV laser beam is focused into the vacuum chamber (waist $\approx$ 50–100 μm) by means of a MgF_2 lens either perpendicular or parallel to the plasma expansion axis, as shown in figure 2. In the latter case the optics are located in the vacuum chamber and protected from the plasma flow by means of a water-cooled screen.

Nitrogen atoms are excited with two 206.7 nm photons from the $2p\,^4S_{3/2}$ ground-state to the $3p\,^4S_{3/2}$ state [1, 23]. The excitation is monitored by detection of the 742–747 nm infrared fluorescence radiation that results from the spontaneous emission to the $3s\,^4P$ manifold. The excited state fluorescence yield is imaged perpendicular to the plan defined by the laser beam and the jet axis onto a slit. The slit ($1 \times 1\,\mathrm{mm}^2$) defines the detection volume of which the dimensions are smaller than any gradient scale length. The infrared radiation is directed towards a gated photomultiplier tube (Hamamatsu R928, 1.5 μs opening time). The continuous background light emitted by the nitrogen plasma is strongly reduced by a 10 nm FWHM interference filter centred at 742 nm. The current delivered by the detector is charge integrated and recorded by means of an ADC connected to a computer. The fluorescence signal is obtained by substracting from the signal acquired during a laser shot the background emission signal measured in between two laser shots. The dye laser frequency is calibrated by recording the absorption spectrum of molecular iodine [20, 22]. An example

of simultaneous recording of the nitrogen laser induced fluorescence light and the I_2 absorption lines is shown in figure 3.

From a spectral scan over the two-photon transition, the local N(^{4}S) atom density, temperature and velocity are determined. Absolute number densities are obtained by calibrating the N(^{4}S) atom fluorescence yield using a well defined amount of krypton gas [1, 24]. Krypton atom has a two-photon excitation scheme very similar to that of nitrogen and the ratio of the two-photon absorption cross-section of Kr to N(^{4}S) has been accurately measured [24]. The temperature is calculated from the Doppler broadening of the spectral line which is the main broadening mechanism under our experimental conditions. The Doppler linewidth is obtained after deconvolution of the measured fluorescence profile with the laser profile which is assumed to be Gaussian [1]. The mean velocity is obtained from the Doppler shift of the fluorescence peak. A systematic error of $\pm 260\,\mathrm{m\,s^{-1}}$ in the velocity arises from the uncertainty in the position of the I_2 absorption peaks that equals $0.015\,\mathrm{cm^{-1}}$. Note that when the laser beam propagates perpendicular, respectively parallel, to the jet centreline, the perpendicular temperature $T_\perp$, respectively the parallel temperature $T_\parallel$, and the radial velocity v_r, respectively the axial velocity v_z, are determined.

Within the barrel and normal shock wave of the plasma expansion the motion is in non-equilibrium and the one-dimensional atom velocity distribution function departs from a Gaussian. Nevertheless, in that case the velocity distribution can be decomposed into two dynamic Gaussian components, as has been shown recently [25–27]: a fast and cold Gaussian component that corresponds to supersonic beam conditions and a slow and warm Gaussian component that corresponds to conditions in the shock region. The medium not being in thermodynamic equilibrium in the shock wave zones, the N(^{4}S) atom mean velocity and temperature have to be directly determined from the measured distribution. The velocity is deduced from the first moment of the distribution. The temperature is calculated from the density weighted temperature of the two Gaussian components of the distribution. In this contribution only the macroscopic properties of the nitrogen atom flow are discussed. Details concerning the behaviour of the N(^{4}S) atom velocity distribution function in the shock region of an expanding nitrogen plasma can be found in [26].

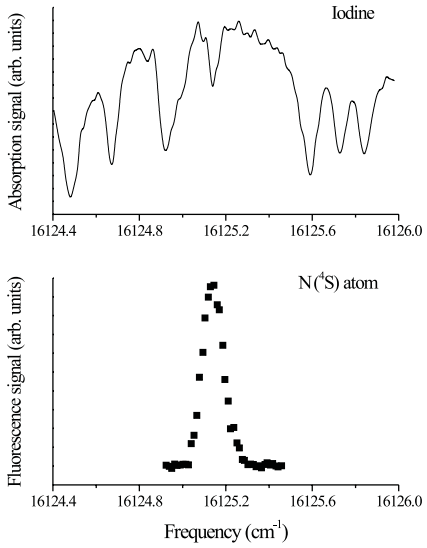

Figure 3. Example of a spectral scan with simultaneous recording of the nitrogen atom 2-photon LIF signal (■) and the I_2 absorption signal (——). The horizontal frequency axis is calibrated by the position of the I_2 absorption lines. Every measured spectral profile is obtained using 300 shots per data point because of the UV beam pulse to pulse energy fluctuation.

4. N(^{4}S) atom flow properties along the jet axis

4.1. Density

The on-axis profile of the ground-state nitrogen atom density is shown in figure 4 for two different background pressures. In the supersonic domain of the expansion and behind $z = 4$ mm, that corresponds to the distance it takes for the jet to open, the N(^{4}S) density decreases quadratically with the axial position z regardless of the pressure. This indicates that the drop in density along the jet centreline is a direct consequence of the increase in the jet diameter [19]. This effect is known as the rarefaction effect. The compression stage through the normal stationary shock wave is clearly visible in figure 4. A compression ratio of 1.7 is found for both background pressures. Using the well-established Rankine–Hugoniot relations [18,19], a Mach number ahead of the shock wave of 1.4 is deduced from the N(^{4}S) atom density jump. This estimated Mach number is about three times less than the one directly obtained from the measurement of the axial velocity, see section 4.3, meaning that the compression effect is somehow attenuated. Furthermore the magnitude of the rise in density across the shock wave does not match the drop in velocity. This disagreement confirms the fact, already implied in the previous remark, that the N(^{4}S) atom forward flux is not conserved across the shock front. In the subsonic domain the density decreases slowly, as can be seen in figure 4, whereas the neutral gas supersonic expansion theory predicts a flow at constant static pressure beyond the shock wave [18–20].

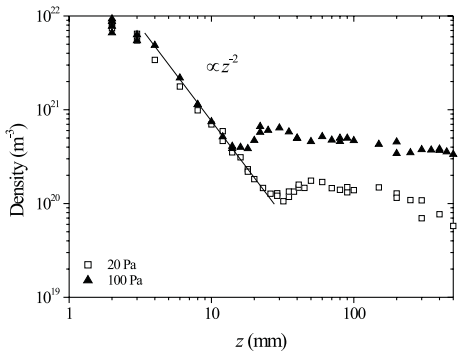

Figure 4. Ground-state nitrogen atom density profile along the jet centreline at 20 Pa (□) and 100 Pa (▲) background pressure. At some distance from the arc nozzle outlet the density decrease is proportional to z^{-2} regardless of the pressure. This is a direct consequence of the rarefaction effect. At 20 Pa the forward flux is not conserved throughout the normal shock wave (too small density jump, see figure 6). The density drop in the subsonic domain results from wall-association of nitrogen atoms.

In order to fulfil the perfect gas law in the subsonic domain, the density should increase since the plasma flow cools down.

Ground-state nitrogen atoms can recombine in volume to form molecular nitrogen according to the following three-particle reactions

$$N + N + N \rightarrow N_2(A, B) + N$$
$$k \approx 1.4 \times 10^{-44}\,m^6\,s^{-1} \quad [28], \tag{4}$$
$$N + N + N_2 \rightarrow N_2(A, B) + N_2$$
$$k \approx 6.8 \times 10^{-46}\,m^6\,s^{-1} \quad [29]. \tag{5}$$

The reaction rates, however, are too low to lead to any significant loss of $N(^4S)$ atoms under our experimental conditions. Therefore, the observed losses of atomic nitrogen in the course of the plasma expansion can only be explained by the existence of an escape path for $N(^4S)$ atoms. The anomalous transport of atomic radicals in supersonic plasma jets has been recently the subject of several communications [20,30,31]. Those studies are mainly focused on the H atom flow characteristics in argon/hydrogen and hydrogen plasma expansions. On the basis of experimental data we demonstrate that the losses of H atoms arises from an outward diffusion phenomenon driven by the existence of a large density gradient between the core of the jet and its vicinity. The low H atom density in the background gas, which is responsible for the diffusion phenomenon, results from the very efficient recombination of H atoms on the reactor walls.

In like manner, the observed departure from the classical expansion picture in the case of nitrogen atoms is understandable in terms of plasma–surface interactions. The too small density jump across the shock wave as well as the decrease in $N(^4S)$ partial static pressure in the subsonic domain both originate from the recombination of $N(^4S)$ atoms at the vessel walls where they form nitrogen molecules. Nitrogen atoms, however, are better confined inside the nitrogen plasma jet than H atoms in hydrogen containing plasma expansions. For instance, there is no significant losses of $N(^4S)$ in the supersonic domain. This gain in confinement results from the combination of several factors. First, the momentum exchange cross-section of N–N_2 collisions is slightly higher than the cross-section of H–H_2 collisions [32] which has consequences on the local mean free path. Second, the high mass of N atoms leads to a low thermal speed in spite of a relatively high temperature in the jet. Third and last, the loss probability of N atoms on a stainless steel surface is quite low for an atomic radical. Currently available values in the literature vary from 7×10^{-2} to 8×10^{-3} [33]. In the case of H atoms the reported loss coefficients values set around 0.2 [31, 34]. The low recombination probability of $N(^4S)$ on metallic surfaces is often explained in the following way [33]. The wall is first covered by a layer of N atoms on top of which a layer of protective molecular nitrogen is quickly formed. The latter prevents N atoms to reach the surface and therefore to recombine. Due to the combination of all those factors, the outward diffusion flux of $N(^4S)$ atoms stays limited and nitrogen atoms are relatively well transported towards the downstream region.

4.2. Perpendicular and parallel temperature

The axial profiles of the $N(^4S)$ atom perpendicular temperature $T_\perp$, associated with the velocity distribution perpendicular to the jet centreline, measured at different pressures are characteristic for a free jet flow, see figure 5. The rapid cooling of the gas in the supersonic domain is due to conversion of thermal energy gained in the source into kinetic energy. The corresponding acceleration of the plasma flow is clearly visible in figure 6. Across the stationary shock wave, the temperature rises as a consequence of collisions. The influence of the pressure upon both the shock wave thickness and position is obvious in figure 5. The slow decrease of $T_\perp$ in the subsonic zone arises from heat transfer to the ambient gas and therefore to the vessel walls.

It is known that the Poisson adiabatic law can be employed to characterize energy transfer in the supersonic region of weakly ionized plasma expansions even if deviation from an adiabatic behaviour has been established [20, 27, 31]. Therefore, the value of the adiabatic exponent γ can be inferred from a logarithmic plot of the perpendicular temperature as a function of the density. We found $\gamma = 1.45 \pm 0.10$ which corresponds to an adiabatic coefficient of a mixture containing about 80% of nitrogen molecules ($\gamma = \frac{7}{5}$ for N_2 molecules since no significant amount of energy is stored in vibrational motion [18]). The best fit to the temperature curve using the Poisson adiabatic law and the estimated γ, see figure 5, gives

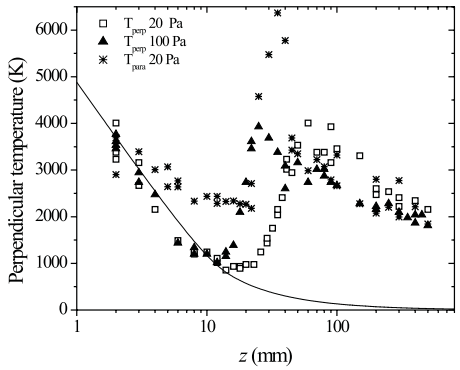

Figure 5. Profile of the nitrogen atom perpendicular temperature $T_\perp$ along the jet axis at 20 Pa (□) and 100 Pa (▲) background pressure. The solid line represents the theoretical perpendicular temperature profile calculated using the Poisson adiabatic law with $\gamma = 1.45$ and $T_o = 8500$ K. Also shown is the axial profile of the nitrogen atom parallel temperature $T_\parallel$ measured at 20 Pa (∗).

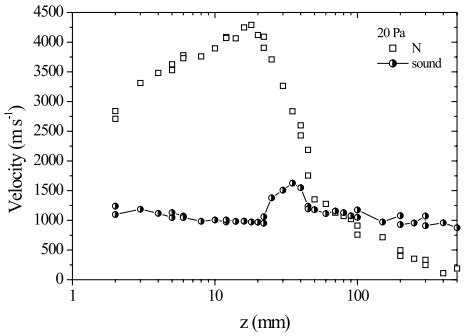

Figure 6. Development of the atomic nitrogen axial velocity component v_z along the plasma jet centreline at 20 Pa background pressure (□). Also shown is the speed of sound c_s calculated from the measured parallel temperature with $\gamma = 1.45$ and $m = 28$ amu (circle). The Mach number M equals 4.4 in front of the normal shock wave. The Mack disc (location at which $M = 1$, i.e. end of the shock wave) is located around $z = 70$ mm.

a temperature of 8500 K at the arc exit. Temperature jumps of 4.1 and 3.9 are measured over the normal shock wave at 20 Pa and 100 Pa, respectively, that corresponds to a Mach number of approximately 4 in both cases according to the Rankine–Hugoniot relation. This value of M agrees with the one deduced from the velocity measurements at 20 Pa.

Also plotted in figure 5 is the axial profiles of the N(^{4}S) atom parallel temperature $T_\parallel$, associated with the velocity distribution parallel to the jet axis, measured at 20 Pa background pressure. The fact that $T_\perp < T_\parallel$ in the final part of the supersonic domain is a direct consequence of geometrical cooling [19]. However, the early deviation from thermal equilibrium as well as the difference in magnitude of the jump accross the shock wave ($M = 3.1$ is deduced from the $T_\parallel$ jump) is not yet understood. The last point, also observed in the case of hydrogen plasma jets [35], certainly finds its origin in the dynamics of a collision event. In the subsonic domain, equilibrium is restored due to numerous collisions.

4.3. Flow velocity and forward flux

The profile of the N(^{4}S) atom axial velocity component v_z measured along the jet centreline at 20 Pa background pressure is shown in figure 6. Also plotted in this graph is the axial profile of the local speed of sound c_s calculated from the measured parallel temperature $T_\parallel$. The frozen speed of sound is given by

$$c_s = \sqrt{\frac{\gamma k_B T}{m}}, \tag{6}$$

where γ is the adiabatic exponent ($\gamma = 1.45$), k_B the Boltzmann constant, and m the mass. We use $m = 28$ amu to determine the sonic speed. The knowledge of both v_z and c_s allows to calculate the local Mach number M, which is an important parameter to distinguish between different flow regimes. Behind the arc exit, the plasma flows supersonically and accelerates due to energy conversion. The normal stationary shock wave, through which directed motion is transformed into thermal motion, stretches from $z = 20$ to 70 mm, as can be seen in figure 6. The end of the shock wave is taken at the Mach disc, i.e. location at which $M = 1$. As expected, the shock wave dimension corresponds to about one local mean free path for N–N_2 collision: $\lambda^{mfp}_{N-N_2} \approx 30$ mm ahead of the shock front at 20 Pa (cross-sections are taken from Phelps [32]). The Mach number equals 4.4 ahead of the normal shock wave, in agreement with the value estimated from the increase in perpendicular temperature in section 4.2.

A parameter of primary importance when this kind of plasma jet is to be used as an atomic radical source is the atom forward flux. The exact form of the radial profile of v_z, being so far unknown, one can only estimate the flux along the jet axis. This gives anyway valuable indications about the potential of such a plasma jet. At the source exit, $z = 2$ mm, the N(^{4}S) atom flux ϕ_N is equal to 2×10^{25} m^{-2} s^{-1}, in front of the normal shock wave $\phi_N = 8 \times 10^{23}$ m^{-2} s^{-1} and behind the shock region $\phi_N = 2 \times 10^{23}$ m^{-2} s^{-1}. The flux of ground-state nitrogen atoms stays high whatever the location in the jet, as can be seen. This kind of reactive particle source has proven to be very efficient in the field of surface modification. For instance, deposition of good quality films has been demonstrated at rates up to 10 nm s^{-1} [36]. Moreover the source delivers particles with a high kinetic energy (E_k(N) $\approx$ 1.2 eV upstream of the shock region) and a relatively low temperature which is favourable for plasma processing and chemistry.

Another way of looking at the chemical potential of this plasma jet is to consider the dissociation degree β. The atomic and molecular fluxes being unknown, β can be obtained in the subsonic domain from the conservation of the static pressure assuming identical temperatures for N and N_2. Just behind the shock wave, one finds $\beta = 33\%$ at 20 Pa ($z = 100$ mm) and $\beta = 20\%$ at 100 Pa ($z = 80$ mm). Taking into account losses in the shock wave, β could be around 40% at the arc exit. In view of the relatively large N(^{4}S) atom fraction, it is likely that such a jet does not contain any N_2(A) molecules [37]. In the background ($z = 500$ mm) one finds $\beta = 4.5\%$ and 5% at 20 Pa and 100 Pa, respectively. It clearly reveals the existence of a loss channel for N(^{4}S) atoms.

5. Radial density, temperature and velocity profiles

A study of the plasma jet cross-section at different distances from the arc outlet, of which the results are shown in figure 7, reveals the detailed structure of the jet. The local density, perpendicular temperature $T_\perp$ and radial velocity component v_r of ground-state nitrogen atoms have been measured as a function of the radial coordinate r at 20 Pa background pressure. The radial profiles have been measured at two different axial positions that corresponds to two well distinct regions: at $z = 10$ mm, i.e. in the supersonic flow domain, and at $z = 25$ mm, i.e. at the start of the stationary normal shock wave.

The sharp rise in temperature, to which corresponds a rapid decrease in velocity, indicates the existence of a stationary barrel shock wave that delimits the zone of silence. Across the barrel shock region, kinetic energy is converted into thermal energy as the result of collisions between particles of the jet and particles located around the jet. One can define a radial Mach number M_r such as $M_r = v_r/c_s$ in order to help visualizing the side shock region. For example, at $z = 10$ mm, the Mach number M_r has its maximum value 2.9 at $r = 5$ mm. This is the start of the barrel shock wave (for obvious symmetry reason we only look at $r > 0$). The shock wave ends at about $r = 15$ mm that corresponds to the position at which $M_r = 1$. In the core of the jet, i.e. in the region of unhampered flow, the temperature is low ($T_\perp < 1000$ K at $z = 10$ mm) due to the adiabatic cooling mechanism. The increase in the magnitude of the radial velocity component is purely a geometric effect [19]. In the vicinity of the jet, the velocity decreases as $|r|$ increases because of collision with the residual background gas to finally reach a value close to zero. Due to the presence of recirculation cells around the jet, the radial velocity is in fact non-zero but it has a value of about 50 m s^{-1} [38]. The TALIF method accuracy, however, is not good enough to access such a low value. Note that because of heat transfer to the vessel walls the gas that surrounds the jet is relatively cold. Also visible in figure 7 is the broadening effect of the jet when moving downstream. The radial structure of the jet is similar to the one described by Bultel *et al* [9] but resolved with a better accuracy.

The shape of the radial density profiles is typical for a consumable species, e.g. identical profiles are observed in the

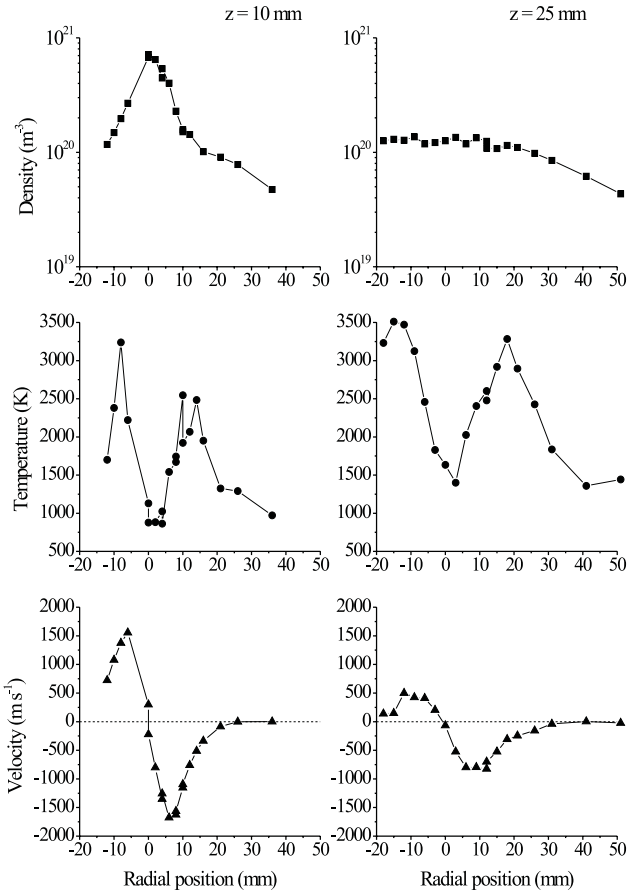

Figure 7. Radial profiles of the density (top), perpendicular temperature $T_\perp$ (middle), and radial velocity v_r (bottom) of N(^{4}S) atoms for a background pressure of 20 Pa at $z = 10$ mm (left) and $z = 25$ mm (right). The barrel shock wave corresponds to the region where $T_\perp$ increases and v_r decreases, i.e. the region where kinetic energy is converted into thermal motion. The outer zone where $T_\perp$ decreases is usually considered as the jet boundary. The two density plots reveal the existence of a N(^{4}S) density gradients between the core of the jet and its surroundings. This density gradient originates from recombination of N(^{4}S) atoms into N_2 molecules at the vessel walls.

case of electrons [39]. The density in the jet is never lower than the density in the background. In other words, there is no sign of any compression effect in the barrel shock wave. As previously explained, this is the result of recombination of N(^{4}S) at the vessel walls. The density gradient responsible for the loss by diffusion can clearly be seen in figure 7.

6. Estimate of the electron density

The radiative lifetime τ of the nitrogen atom $3p\,^4S_{3/2}$ state has been measured using a fast PMT with a single photon response of 1.3 ns (Hamamatsu R5600P-01). Such a measurement is a necessary step in the TALIF set-up calibration procedure in order to obtain absolute number densities [1]. The values of τ, obtained after deconvolution with the laser beam temporal profile (Gaussian shape, FWHM = 5.3 ns), are shown as a function of the axial position in figure 8. The natural radiative lifetime τ_n of the $3p\,^4S_{3/2}$ state is found to be 27.3 ± 1.1 ns in good agreement with the value of 26.2 ± 1.5 ns given in the literature [1].

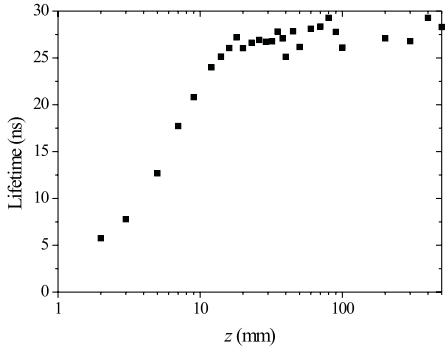

Figure 8. The radiative lifetime of the nitrogen atom $3p\,^4S_{3/2}$ state as a function of the position along the jet axis at a background pressure of 20 Pa. In the first few millimetres of the expansion ($z < 20$ mm) the lifetime of the nitrogen atom excited state is controlled by electron impact. The natural radiative lifetime of the $3p\,^4S_{3/2}$ state is found to be 27.3 ± 1.1 ns in agreement with the value of 26.2 ± 1.5 ns reported in literature [1].

The short decay time observed at low z ($z < 20$ mm) arises from de-excitation by collisions, i.e. quenching. In the supersonic domain, the main plasma constituents are N_2 molecules, N atoms, N^+ ions and electrons. The quenching rate of excited nitrogen atom by N(^{4}S) atoms is assumed not to be larger than the quenching rate by N_2 molecules which is equal to 4.1×10^{-17} m^3 s^{-1} [24]. Even supposing a N_2 density at the arc exit as high as 6×10^{22} m^{-3}, the rate coefficient is far too low to explain the very short lifetime of the $3p\,^4S_{3/2}$ state. Furthermore de-excitation by N^+ impact can be neglected [40]. Collisions with electrons then appear to be the only way of explaining the short radiative lifetime. Consequently, τ can be written as follows:

$$\tau = \frac{1}{1/\tau_n + k_e n_e}, \tag{7}$$

where k_e is the electron quenching rate coefficient. Thus it appears that the electron density can be extracted from the lifetime measurements. To the best of our knowledge the value of the electron quenching rate of the $3p\,^4S_{3/2}$ state for low electron energy has never been reported in the literature. Therefore we choose to follow the geometrical approach for cold collision proposed by Van der Mullen [41] in order to estimate k_e. The rate coefficient can to first order be approximated by

$$k_e \approx \sigma v_e, \tag{8}$$

where σ is the mean electron impact de-excitation cross-section and v_e is the electron thermal speed. Using the cross-section expression derived in [41] one obtains

$$k_e \approx 4\pi a_0^2 n^4 v_e = 4\pi a_0^2 n^4 \left(\frac{3k_B T_e}{m_e}\right)^{1/2}, \tag{9}$$

where a_0 is the Bohr radius, n is the principal quantum number, k_B is the Boltzmann constant and m_e the rest mass of the electron. The local electron density can be obtained from the measured radiative lifetime using equations (7) and (9), assuming $T_e = T_N$ in the jet. This assumption is reasonable due to the efficient energy coupling between electrons and heavy particles under free plasma jet conditions. For instance, in argon jets one observes $T_e \approx T_{neutrals}$ [27,42]. The axial profile

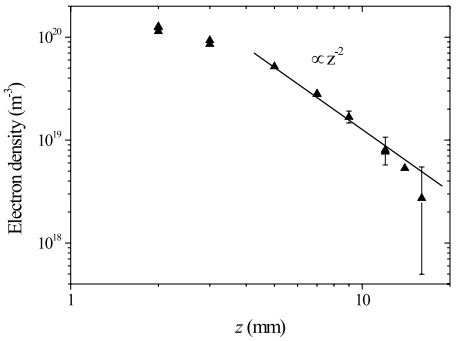

Figure 9. Axial profile of the electron density at 20 Pa background pressure as obtained from the measured nitrogen atom excited state lifetime. The valuation of the de-excitation rate by electron impact is based upon a geometrical cross-section [41]. Also shown is the expected electron density asymptotic behaviour (——) ensuing from the rarefaction effect. The error bars reflect the uncertainty in the nitrogen atom excited state natural lifetime.

of the electron density in the first millimetres of the expansion is shown in figure 9. At the nozzle outlet, $z = 2$ mm, the electron density is relatively high, $n_e = 10^{20}\,m^{-3}$, that corresponds to an ionization degree of about 1%. The estimated electron density agrees with the value measured by Langmuir probe in a supersonic nitrogen plasma jet generated from a dc arc equipped with a convergent–divergent nozzle [7]. An upper limit for the electron density at the arc exit can be given from Stark effect data [40]. Since neither Stark broadening nor Stark shift have been noticed, n_e cannot exceed $10^{21}\,m^{-3}$. All this supports the validity of the geometrical approximation of the electron quenching rate coefficient. In the supersonic domain, the decrease of n_e is proportional to z^{-2}. The latter therefore originates from the rarefaction effect. It shows that recombination processes have little influence on electron and ion losses during the supersonic stage of the expansion [18]. Knowing the shock wave position and thickness, the electron density in the subsonic region can be roughly estimated using the free jet flow theory. We obtain $n_e \approx 4 \times 10^{18}\,m^{-3}$. Under such conditions, N^+ ion is the main ion in the plasma jet. Indeed at high electron density the dissociative recombination of N_2^+ molecular ions is very fast whereas N^+ ions are destroyed by charge exchange or by 3-particle recombination which are slow processes in comparison. Note that the charge exchange reaction between N^+ and $N_2(A)$ is also an efficient channel for destruction of $N_2(A)$ molecules [43].

7. Conclusion

The study of macroscopic flow properties of ground-state nitrogen atoms using a TALIF diagnostic technique reveals that free nitrogen plasma jets have to be considered as an efficient $N(^4S)$ source. The high chemical potential of such jets, in term of $N(^4S)$ contents, combined with a low temperature and a high particle kinetic energy make them a suitable tool for surface treatment applications in which $N(^4S)$ atoms play a dominant role, e.g. deposition of thin N-containing semiconductor layers. As expected in light of earlier experiments performed on hydrogen plasma expansions, the transport of $N(^4S)$ atoms within a jet is influenced by recombination processes taking place at walls. Part of the nitrogen atoms escape the plasma jet, and thus they do not contribute to the chemistry in the downstream region. However, losses in the core of the plasma flow are limited due to the relatively high N atom mass and due to the low N atom surface recombination probability. By improving the source fragmentation capability and by minimizing losses playing with the wall material, a $N(^4S)$ atom flux upstream of the normal shock front as high as several times $10^{24}\,m^{-2}\,s^{-1}$ can certainly be achieved. Another interesting approach to develop a versatile $N(^4S)$ atom source is to use an Ar/N_2 mixture. Preliminary investigations of plasma jets generated from such a mixture have already given promising outcomes [44]. In that case, $N(^4S)$ atom production is favoured by a fast charge exchange reaction between Ar^+ and N_2. Furthermore the high Ar–N collision cross-section leads to an efficient trapping of $N(^4S)$ atom inside the jet. Finally, such a plasma may also be of interest when ions are needed for the overall chemical process.

Acknowledgments

The authors greatly appreciate the skilful technical assistance of M J F van de Sande, A B M Hüsken and H M M de Jong. This work is part of the research program of the Dutch Foundation for Fundamental Research on Matter (FOM) via project 95RG09. It is financially supported by the Dutch Organization for Scientific Research (NWO) as well as the Euratom foundation.

References

[1] Mazouffre S, Foissac C, Supiot P, Vankan P, Engeln R, Schram D C and Sadeghi N 2001 *Plasma Sources Sci. Technol.* **10** 168
[2] Schönemann A T, Lago V and Dudeck M 1996 *J. Therm. Heat Transfer* **10** 419
[3] Mitcheltree R A 1991 *J. Spacecraft* **28** 619
[4] Nakamura S, Mukai T and Senoh M 1994 *J. Appl. Phys.* **76** 8189
[5] Orton J W and Foxon C T 1998 *Rep. Prog. Phys.* **61** 1
[6] Aberle A G 2001 *Solar Energy Mater.* **65** 239
[7] Robin L, Vervisch P and Cheron B G 1994 *Phys. Plasmas* **1** 444
[8] Domingo P, Bourdon A and Vervisch P 1995 *Phys. Plasmas* **2** 2853
[9] Bultel A, Chéron B G and Vervisch P 1995 *Plasma Sources Sci. Technol.* **4** 597
[10] Broc A, Dilecce G and De Benedictis S 2001 *Proc. 4th Frontiers in Low Temperature Plasma Diagnostics (Rolduc, The Netherlands)* p 79
[11] De Benedictis S, Dilecce G, Simek M and Vigliotti M 1998 *Plasma Sources Sci. Technol.* **7** 557
[12] Douai D, Berndt J and Winter J 2002 *Plasma Sources Sci. Technol.* **11** 60
[13] Kroesen G M W, Schram D C and de Haas J C M 1990 *Plasma Chem. Plasma Process.* **10** 551
[14] Brown S C 1966 *Basic Data of Plasma Physics* (Cambridge, MA: MIT Press)
[15] Guerra V and Loureiro J 1997 *Plasma Sources Sci. Technol.* **6** 361
[16] Sá P A and Loureiro J 1997 *J. Phys. D: Appl. Phys.* **30** 2320
[17] Gordiets B, Ferreira C M, Pinheiro M J and Ricard A 1998 *Plasma Sources Sci. Technol.* **7** 363
[18] Schram D C, Mazouffre S, Engeln R and van de Sanden M C M 2001 *Atomic and Molecular Beams* ed R Campargue (New York: Springer) p 209

[19] Miller D R 1988 *Atomic and Molecular Beam Methods* ed G Scoles (New York: Oxford University Press) p 14
[20] Mazouffre S, Boogaarts M G H, Bakker I S J, Vankan P, Engeln R and Schram D C 2001 *Phys. Rev.* E **64** 016411
[21] Czarnetzki U, Miyazaki K, Kajiwara T, Muraoka K, Maeda M and Döbele H F 1994 *J. Opt. Soc. Am.* B **11** 2155
[22] Boogaarts M G H, Mazouffre S, Brinkman G J, van der Heijden H W P, Vankan P, van der Mullen J A M, Schram D C and Döbele H F 2002 *Rev. Sci. Instrum.* **73** 73
[23] Adams S F and Miller T A 1998 *Chem. Phys. Lett.* **295** 305
[24] Niemi K, Schultz von der Gathen V and Döbele H F 2001 *J. Phys. D: Appl. Phys.* **34** 2330
[25] Mazouffre S, Vankan P, Engeln R and Schram D C 2001 *Phys. Rev.* E **64** 066405
[26] Mazouffre S, Vankan P, Bakker I, Engeln R and Schram D C 2001 *Proc. 10th Laser-Aided Plasma Diagnostics (Fukuoka, Japan)* p 424, available on-line at www.etp.phys.tue.nl
[27] Engeln R, Mazouffre S, Vankan P, Schram D C and Sadeghi N 2001 *Plasma Sources Sci. Technol.* **10** 595
[28] Chen Sin-Li and Gooding J M 1969 *J. Chem. Phys.* **50** 4335
[29] Gordiets B F, Ferreira C M, Guerra V L, Loureiro J M A H, Nahorny J, Pagnon D, Touzeau M and Vialle M 1995 *IEEE Trans. Plasma Sci.* **23** 750
[30] Mazouffre S, Boogaarts M G H, van der Mullen J A M and Schram D C 2000 *Phys. Rev. Lett.* **84** 2622
[31] Mazouffre S, Vankan P, Engeln R and Schram D C 2001 *Phys. Plasma* **8** 3824
[32] Phelps A V 1990 *J. Phys. Chem. Ref. Data* **19** 653 (for H–H_2 collisions)
Phelps A V 1991 *J. Phys. Chem. Ref. Data* **20** 557 (for N–N_2 collisions)
[33] Singh H, Coburn J W and Graves D B 2000 *J. Appl. Phys.* **88** 3748
Adams S F and Miller T A 2000 *Plasma Sources Sci. Technol.* **9** 248
[34] Kae-Nume P, Perrin J, Jolly J and Guillon J 1996 *Surf. Sci.* **360** L495
[35] Mazouffre S 2001 *PhD Thesis* Eindhoven University of Technology, The Netherlands, p 81, available on-line at www.tue.nl/bib/indexen.html
[36] Kessels W M M, Van de Sanden M C M and Schram D C 2000 *J. Vac. Sci. Technol.* A **18** 2153
[37] Cernogora G, Ferreira C M, Hochard L, Touzeau M and Loureiro J 1984 *J. Phys. B: At. Mol. Phys.* **17** 4429
[38] Selezneva S E, Boulos M I, van de Sanden M C M, Engeln R and Schram D C 2002 *J. Phys. D: Appl. Phys.* **35** 1362
[39] Meulenbroeks R F G, Engeln R A H, Beurskens M N A, Paffen R M J, van de Sanden M C M, van der Mullen J A M and Schram D C 1995 *Plasma Sources Sci. Technol.* **4** 74
[40] Griem H R 1969 *Spectral Line Broadening by Plasmas* (London: Academic)
[41] Van der Mullen J A M 1990 *Phys. Rep.* **191** 110
[42] Van de Sanden M C M, de Regt J M and Schram D C 1994 *Plasma Sources Sci. Technol.* **3** 501
[43] Brussaard G J H, Aldea E, van de Sanden M C M, Dinescu G and Schram D C 1998 *Chem. Phys. Lett.* **290** 379
[44] Bakker I 2001 *Internal Report* VDF/NT 01-06, Eindhoven University of Technology, The Netherlands